

# The role of elasticity in the formation of electrospun fibers

Jian H. Yu, Sergey V. Fridrikh, Gregory C. Rutledge\*

*Department of Chemical Engineering, Massachusetts Institute of Technology, 77 Massachusetts Avenue, Cambridge, MA 01239, USA*

Received 7 February 2006; accepted 19 April 2006

## Abstract

The role of fluid elasticity in the formation of fibers from polymer solution by electrospinning is investigated. Model solutions with different degrees of elasticity were prepared by blending small amounts of high molecular weight polyethylene oxide (PEO) with concentrated aqueous solutions of low molecular weight polyethylene glycol (PEG). The elastic properties of these solutions, such as extensional viscosity and the longest relaxation time, were measured using the capillary breakup extensional rheometer (CaBER). The formation of beads-on-string and uniform fiber morphologies during electrospinning was observed for a series of solutions having the same polymer concentration, surface tension, zero shear viscosity, and conductivity but different degrees of elasticity. A high degree of elasticity is observed to arrest the breakup of the jet into droplets by the Rayleigh instability and in some cases to suppress the instability altogether. We examine the susceptibility of the jet to the Rayleigh instability in two ways. First, a Deborah number, defined as the ratio of the fluid relaxation time to the instability growth time, is shown to correlate with the arrest of droplet breakup, giving rise to electrospinning rather than electrospraying. Second, a critical value of elastic stress in the jet, expressed as a function of jet radius and capillary number, is shown to indicate complete suppression of the Rayleigh instability and the transition from ‘beads-on-string’ to uniform fiber morphology.

© 2006 Elsevier Ltd. All rights reserved.

*Keywords:* Electrospinning; Elasticity; Boger fluid

## 1. Introduction

Electrospinning is a process that employs electrostatic forces to produce fibers with diameters ranging from a few microns to tens of nanometers. Recently, electrospun fibers have attracted great attention due to their potential applications in nanocomposites [1,2], biomedical engineering [3,4], protective clothing [5], sensors [6,7], magneto-responsive fibers [8], and superhydrophobic membranes [9,10]. In at least one case, the performance of the resulting material was shown to depend strongly on fiber morphology [11].

Although the process of electrospinning is relatively easy to implement, many polymer solutions are not readily electrospun into the uniform fibers usually desired. Electrospinning of uniform fibers can become problematic when the polymer solution is too dilute, due to limited solubility of the polymer, for example, or when the polymer chains are either short or rigid [12]. In these cases, experience suggests that the lack of elasticity of the solution prevents the formation of uniform

fibers; instead, droplets or necklace-like structures known as ‘beads-on-string’ are formed [13–15]. The common remedy for this problem is to formulate the spin solution with a second polymer whose purpose is to impart greater elasticity to the solution, rendering it electrospinnable [16,17]. The added polymer may form a network of entanglements, making the solution more elastic and electrospinnable into uniform fibers. For this to happen, the polymer concentration should be well above the critical overlap concentration,  $c^*$ . The link between the formation of entanglements in solution and their electrospinnability has been established previously [18–21]. However, the presence of entanglements is a sufficient but not a necessary condition for the polymer fluid to demonstrate strong elastic properties. The elastic response can also be achieved at lower polymer concentration if the relaxation time of the fluid is longer than the time of extensional deformation. This kind of elastic behavior is typical of Boger fluids that show high elasticity at concentrations well below  $c^*$  [22,23].

The formation of droplets and the ‘beads-on-string’ morphology in electrospinning has a lot in common with the phenomenon of laminar jet breakup due to surface tension [24–26]. A Newtonian liquid jet breaks into droplets due to the Rayleigh instability driven by the surface tension forces. To the contrary, a viscoelastic jet tends to take longer time to break up or does not break up at all, forming a ‘beads-on-string’

\* Corresponding author. Tel.: +1 617 253 0171; fax: +1 617 253 8992.  
E-mail address: [rutledge@mit.edu](mailto:rutledge@mit.edu) (G.C. Rutledge).

structure or preserving its uniformity. The build up of the extensional stress stabilizes the jet and retards or arrests the Rayleigh instability. This extensional stress in the jet determines the final breakup mechanism [26]. A linear stability analysis of electrically forced jets has been performed to illuminate the competition between different modes of instability in an electrified fluid jet [27–31]. Hohman et al. predicted three competing instabilities: the Rayleigh mode, a new, axisymmetric conducting mode, and the whipping mode (sometimes called ‘bending’ mode) [27]. The dominant mode of instability depends on the material properties of the fluid and on the operating parameters of the process. Reneker et al. have modeled the whipping mode as an Earnshaw type instability due to electrostatic repulsion, stabilized by surface tension and viscoelastic forces [29]. It is noteworthy that the whipping mode can exist in the absence of viscoelasticity and other competing modes can take place simultaneously, as is the case for an electrified water jet [32,33]. Regardless whether the electrified jet consists of a Newtonian fluid or a viscoelastic fluid, if the Rayleigh break-up instability is not suppressed, the jet can result in a ‘beads-on-string’ structure and ultimately breaks up into droplets.

The influences of numerous solution properties, including shear viscosity, polymer concentration, solution conductivity, and surface tension, on fiber morphology have been investigated experimentally [13–15,34]. Although researchers have recognized the important role of elasticity in electrospinning [15,20,31,35,36], its impact on the fiber morphology has not been studied systematically due to the difficulty of maintaining other solution properties constant while changing the elasticity. In a study by Theron et al., the fluid relaxation time was measured, but no conclusion regarding the role of the elasticity was drawn [35]. Gupta et al. used the dimensionless quantity  $c[\eta]$  (where  $c$  is the polymer concentration in solution and  $[\eta]$  is the intrinsic viscosity) to describe fluid elasticity, and studied the formation of electrospun fibers in three different concentration regimes (dilute, semi-dilute, concentrated) [15]. In this paper, we present a study of several series of polymer solutions that have the same shear viscosity, concentration, conductivity, and surface tension, but different degrees of elasticity, in order to isolate and reveal the role of elastic effects in electrospinning.

## 2. Experimental section

Liquids with constant shear viscosity and different degrees of elasticity are known as Boger fluids [22]. In this study, the test fluids are aqueous analogs of Boger fluids developed by Dontula et al. [23]. Poly(ethylene oxide) (PEO) and poly(ethylene glycol) (PEG) of various molecular weights were purchased from the Aldrich Chemical Co. Molecular weights were determined by gel permeation chromatography. The weight average molecular weights (g/mol) of the PEO samples used were: 672 k, 772 k, 920 k, 954 k and 1030 k. For PEG, the molecular weight was 10 k. All chemicals were used as received without further purification. Appropriate amounts of PEO were first dissolved in de-ionized water to make a very

dilute solution, and then PEG was added to the solution. Several series of solutions with the same PEO and PEG concentrations but with PEO of different molecular weights were made. Porter and Johnson reported an entanglement transition for molten PEG at an average molecular weight  $M_c = 10$  k g/mol (determined by viscosity–shear correlation) [37]. Simply correcting for dilution the critical concentration for chain entanglement in solution,  $c^* = (M_c \rho) / M$  (where  $\rho$  is the density of PEO) [21], lies above 1 wt% for all of the molecular weights used here. Alternatively,  $c^*$  can be estimated using  $c^* = 3M / (4\pi N_A R_g^3)$ , where  $N_A$  is the Avogadro number, and knowledge of the dependence of the radius of gyration  $R_g$  on molecular weight  $M$  for PEO in a solution of PEG and water. For dilute solutions of PEO in water,  $R_g = 0.215M^{0.583}$  (Å) [38]. For the PEO molecular weights used here,  $c^*$  determined by this method lies between 0.12 and 0.17 wt%, and around 4% for PEG. However, the solvent quality of the PEG/water solutions used here is not as good as that of pure water [23], so these critical concentrations would all be shifted significantly upwards towards higher concentrations in the current work. Most importantly, however, all of the solutions used here were devoid of any entanglement transition and completely Newtonian when tested in shear. Addition of small amounts of PEO imparts elasticity to the PEG solutions, which are otherwise inelastic. The relatively high concentration of PEG masks the viscous contributions of PEO so that the solutions employed here are non-shear-thinning and the shear viscosity is entirely Newtonian. This makes it possible to control the shear and extensional viscosities of the solutions used in this work independently.

The electrospinning apparatus consisted of two parallel aluminum disks (12 cm diameter) at a separation of up to 1 m, arranged in a vertical configuration. The disks serve to provide a uniform electric field and prevent corona discharge at the spinneret. A stainless steel capillary tube (1.6 mm OD, 1 mm ID) (the ‘spinneret’), was inserted through the center of the upper disk (7 mm protrusion length). A Teflon<sup>®</sup> feedline connected the stainless steel capillary tube to a syringe that was filled with solution. A syringe pump (Harvard Apparatus PHD 2000) controlled the feed rate to the stainless steel capillary tube. A power supply (Gamma High Voltage Research ES-30P) was connected to the upper disk to provide the driving potential. An adjustable insulated stand was used to support the lower disk (the ‘collector’). A 1.0 MΩ resistor connecting the lower disk and the grounding wire provided the voltage drop required to measure the small currents observed during electrospinning. A digital multimeter (Fluke 85 III) was used to measure the voltage drop between the disk and the ground, which was then converted to current using Ohm’s law.

The lower disk was positioned at a sufficient distance (35–50 cm) from the spinneret such that the fibers formed were dry when they hit the collector. The strength of the electric field was adjusted to obtain steady state jetting, such that the pulling rate was not too fast or too slow to cause interruption of the jetting, and the whipping instability persisted. Some PEO/PEG solutions can be electrospun over a wide range of flow rates (0.01–2 ml/min), but others have a relatively narrow operating

window. In this study, we fixed the flow rate at 0.025 ml/min, which was the minimum workable flow rate for all the solutions.

The profile of the straight jet during electrospinning before the onset of instability was captured with a digital camera (Nikon D70) that was fitted with a macro-lens system (either a BALPRO 1 system from NOVOFLEX or a K2 lens from Infinity) and mounted on an adjustable tripod with laser positioning. The combined primary and digital magnification was  $1500\times$ . Fig. 1 shows a photograph of the jet near the nozzle and the subsequent image after processing to reveal the profile of the jet. Additional images of the jet taken at successively greater distances from the nozzle were combined to form a composite image of the jet complete from the nozzle to the onset of instability. The jet diameter as a function of position was obtained using image processing software (Image-J, National Institutes of Health, <http://rsb.info.nih.gov/ij/>).

Surface tension measurements were performed using a tensiometer (Kruss-10). The electrical conductivity of the fluids was measured using a conductivity meter (Cole-Parmer-19820). Shear viscosity measurements were performed in a cone-plate viscometer (TA Instruments AR2000). Scanning electron microscopy (JOEL SEM 6320) was used to observe the fiber morphology. Each sample was coated with a layer (10 nm thick) of gold before observation.

A capillary breakup extensional rheometer (Thermo Haake CaBER 1) was used to characterize the extensional properties of the solution. The CaBER is a filament-stretching device that monitors the diameter at the mid-point of a fluid filament as it

thins under action of the capillary force. The Hencky strain,  $\varepsilon$ , and the apparent extensional viscosity,  $\eta_{\text{ext}}$ , are defined as follows [39–41]

$$\varepsilon = 2 \ln \left( \frac{D_0}{D_{\text{mid}}(t)} \right) \quad (1)$$

$$\eta_{\text{ext}} = \frac{\sigma}{-d(D_{\text{mid}}(t))/dt} \quad (2)$$

where  $D_0$  is the initial diameter of the unstretched fluid filament,  $D_{\text{mid}}(t)$  is the time-dependent diameter of the stretched fluid filament at the mid-point, and  $\sigma$  is the surface tension. The CaBER 1 can measure Hencky strains up to 12.7. The time evolution of  $D_{\text{mid}}(t)$  data can be modeled using the following equation [41]

$$D_{\text{mid}}(t) = D_1 \left( \frac{D_1 G}{4\sigma} \right)^{1/3} e^{(-t/3\lambda_p)} \quad (3)$$

where  $G$  is the elastic modulus,  $D_1$  the initial midpoint diameter just after stretching, and  $\lambda_p$  the characteristic time scale of viscoelastic stress growth in uniaxial elongational flow, henceforth called the fluid relaxation time. The above equation stems from the balance between the capillary forces, which create extra pressure on the surface of the uniform cylindrical jet and cause it to extend uniaxially, and viscoelasticity, which resists the deformation caused by the capillary forces.

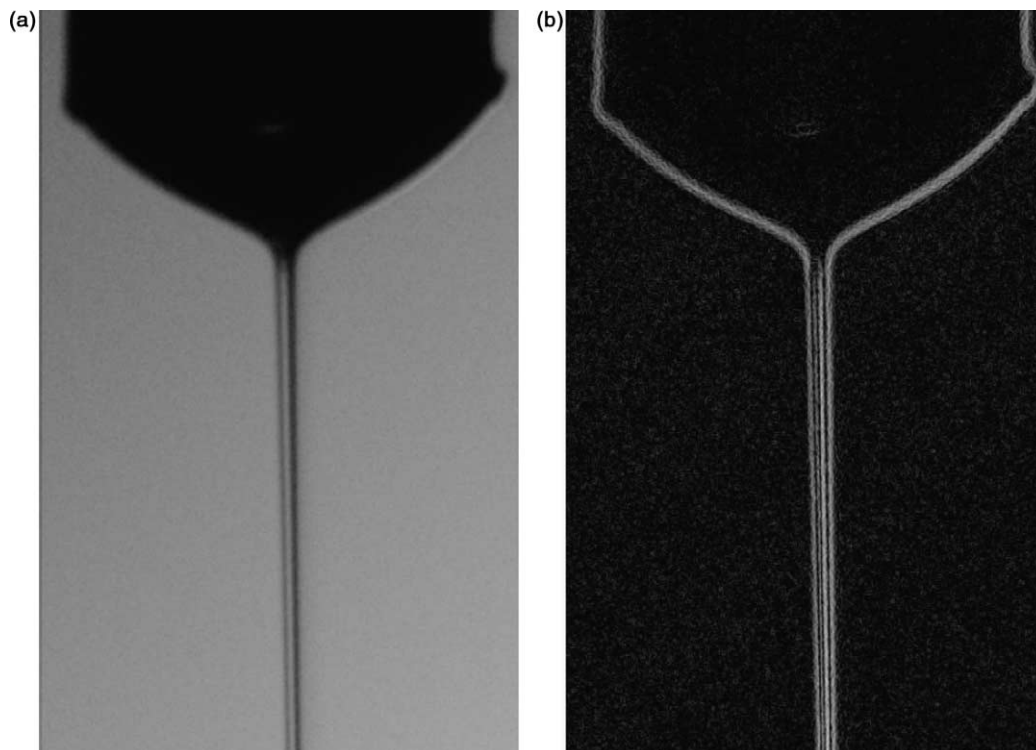


Fig. 1. Photograph of the jet near the nozzle. (The nozzle diameter is 1.6 mm). (a) Actual photographic image. (b) Subsequent image after processing to reveal the profile of the jet.

### 3. Results and discussion

#### 3.1. Solution characterization

Eight series of PEO/PEG solutions with concentrations ranging from 8 to 42 wt% PEG and 0.1 to 0.2 wt% PEO were prepared. These solutions were characterized as reported in Table 1. Fig. 2 is a typical plot of shear viscosity versus shear rate for three of these series of solutions. This plot and others like it confirm that all of our solutions behave like Newtonian fluids, with shear viscosities being independent of the shear rate. Within each series of solutions, the average shear viscosity does not vary by more than 0.05 Pa s. The surface tensions of all solutions are in the narrow range of 52–61 mN/m; the surface tension declines slightly at higher concentrations of PEG. The conductivities all fall within the

relatively narrow range of 49–56  $\mu\text{S}/\text{cm}$  as well. The extensional properties were obtained from the time evolution of the fluid filament diameter in the CaBER. Fig. 3(a) shows the results of the filament diameter evolution for one of the series (Series B1) of PEO/PEG solution. The relaxation times of the fluids were determined from numerical fits to the filament diameter in the range of exponential thinning, as shown in Fig. 3 (a). The plots of apparent extensional viscosity as a function of Hencky strain indicate that the strain hardening effect is more pronounced for solutions containing higher molecular weight PEO. Fig. 3 (b) shows the dramatic increase in the apparent extensional viscosity with Hencky strain. An increase in the molecular weight of PEO does not change the shear viscosity significantly. Meanwhile, the relaxation time and the extensional viscosity can increase by two and three orders of magnitude, respectively. For PEG solutions without

Table 1  
Solution properties and fiber morphologies of PEO/PEG solutions

| Sample series and concentrations | PEO $M_w$ (g/mol) | Relaxation time (s) | Elastic modulus $G$ (Pa) | Extensinal stress at $h_1$ (Pa) | Average shear viscosity (Pa s) | Surface tension (mN/M) | Conductivity ( $\mu\text{S}/\text{cm}$ ) | Fiber morphology (fiber diameter, $\mu\text{m}$ ) |
|----------------------------------|-------------------|---------------------|--------------------------|---------------------------------|--------------------------------|------------------------|--|---|
| A1:                              | 672,000           | 0.016               | 6.2                      | 262                             | 0.096                          | 57.2                   | 54.3                                     | Beads-on-string                                   |
| 32 wt% PEG                       | 772,000           | 0.044               | 1.8                      | 552                             | 0.093                          | 58.6                   | 53.6                                     | Beads-on-string                                   |
| 0.1 wt% PEO                      | 920,000           | 0.072               | 2.1                      | 325                             | 0.099                          | 57.3                   | 55.4                                     | Beads-on-string                                   |
|                                  | 954,000           | 0.10                | 2.9                      | 565                             | 0.097                          | 55.5                   | 54.9                                     | Uniform (2.7)                                     |
|                                  | 1,030,000         | 0.26                | 1.0                      | 540                             | 0.100                          | 56.3                   | 55.2                                     | Uniform (3.4)                                     |
| A2:                              | 672,000           | 0.025               | 3.6                      | 298                             | 0.090                          | 58.5                   | 53.4                                     | Beads-on-string                                   |
| 32 wt% PEG                       | 772,000           | 0.054               | 2.5                      | 859                             | 0.102                          | 55.7                   | 56.3                                     | Beads-on-string                                   |
| 0.2 wt% PEO                      | 920,000           | 0.11                | 3.7                      | 479                             | 0.100                          | 57.6                   | 53.3                                     | Fiber, few beads                                  |
|                                  | 954,000           | 0.16                | 2.8                      | 276                             | 0.116                          | 57.1                   | 52.8                                     | Uniform (5.1)                                     |
|                                  | 1,030,000         | 0.29                | 1.4                      | 212                             | 0.123                          | 58.0                   | 54.2                                     | Uniform (6.6)                                     |
| B1:                              | 672,000           | 0.023               | 5.4                      | 619                             | 0.134                          | 56.7                   | 53.9                                     | Beads-on-string                                   |
| 37 wt% PEG                       | 772,000           | 0.046               | 2.1                      | 588                             | 0.141                          | 56.2                   | 56.2                                     | Beads-on-string                                   |
| 0.1 wt% PEO                      | 920,000           | 0.077               | 2.5                      | 847                             | 0.141                          | 54.6                   | 54.3                                     | Beads-on-string                                   |
|                                  | 954,000           | 0.13                | 2.7                      | 759                             | 0.146                          | 55.0                   | 53.2                                     | Uniform (3.1)                                     |
|                                  | 1,030,000         | 0.27                | 1.8                      | 1422                            | 0.133                          | 53.9                   | 55.6                                     | Uniform (2.7)                                     |
| B2:                              | 672,000           | 0.037               | 3.4                      | 428                             | 0.161                          | 55.3                   | 53.4                                     | Beads-on-string                                   |
| 37 wt% PEG                       | 772,000           | 0.11                | 1.8                      | 639                             | 0.150                          | 55.9                   | 53.5                                     | Uniform (2.6)                                     |
| 0.2 wt% PEO                      | 920,000           | 0.14                | 1.6                      | 584                             | 0.159                          | 54.1                   | 56.7                                     | Uniform (4.4)                                     |
|                                  | 954,000           | 0.21                | 1.6                      | 266                             | 0.167                          | 53.1                   | 51.2                                     | Uniform (8.9)                                     |
|                                  | 1,030,000         | 0.29                | 2.6                      | 359                             | 0.176                          | 54.2                   | 55.6                                     | Uniform (8.9)                                     |
| C1:                              | 672,000           | 0.034               | 4.2                      | 593                             | 0.242                          | 52.3                   | 53.5                                     | Beads-on-string                                   |
| 42 wt% PEG                       | 772,000           | 0.080               | 1.6                      | 1001                            | 0.230                          | 52.9                   | 54.5                                     | Beads-on-string                                   |
| 0.2 wt% PEO                      | 920,000           | 0.10                | 2.9                      | 471                             | 0.216                          | 54.2                   | 52.1                                     | Fiber, few beads                                  |
|                                  | 954,000           | 0.16                | 2.7                      | 524                             | 0.236                          | 53.2                   | 53.8                                     | Uniform (2.7)                                     |
|                                  | 1,030,000         | 0.28                | 2.4                      | 760                             | 0.230                          | 51.0                   | 54.8                                     | Uniform (3.1)                                     |
| C2:                              | 672,000           | 0.049               | 5.3                      | 357                             | 0.259                          | 52.6                   | 53.1                                     | Beads-on-string                                   |
| 42 wt% PEG                       | 772,000           | 0.15                | 1.8                      | 298                             | 0.270                          | 55.7                   | 53.6                                     | Uniform (3.6)                                     |
| 0.2 wt% PEO                      | 920,000           | 0.18                | 2.2                      | 782                             | 0.273                          | 53.1                   | 54.0                                     | Uniform (4.1)                                     |
|                                  | 954,000           | 0.21                | 2.8                      | 5972                            | 0.295                          | 53.2                   | 52.9                                     | Uniform (4.3)                                     |
|                                  | 1,030,000         | 0.56                | 2.3                      | 10,000                          | 0.252                          | 52.7                   | 54.3                                     | Uniform (9.5)                                     |
| D1:                              | 672,000           | NA                  | NA                       | NA                              | 0.02                           | 61.4                   | 51.1                                     | Beads-on-string                                   |
| 20 wt% PEG                       | 772,000           | 0.017               | 3.0                      | 124                             | 0.02                           | 61.6                   | 51.5                                     | Beads-on-string                                   |
| 0.1 wt% PEO                      | 920,000           | 0.029               | 1.6                      | 524                             | 0.02                           | 61.1                   | 50.1                                     | Beads-on-string                                   |
|                                  | 954,000           | 0.067               | 1.4                      | 205                             | 0.02                           | 60.0                   | 51.2                                     | Beads-on-string                                   |
|                                  | 1,030,000         | 0.10                | 1.6                      | 295                             | 0.03                           | 60.5                   | 52.8                                     | Uniform (3.2)                                     |
| D1:                              | 672,000           | NA                  | NA                       | NA                              | 0.01                           | 62.6                   | 49.2                                     | Beads-on-string                                   |
| 8 wt% PEG                        | 772,000           | NA                  | NA                       | NA                              | 0.01                           | 63.1                   | 50.3                                     | Beads-on-string                                   |
| 0.1 wt% PEO                      | 920,000           | -0.01               | NA                       | NA                              | 0.01                           | 62.9                   | 50.1                                     | Beads-on-string                                   |
|                                  | 954,000           | 0.031               | 2.5                      | 315                             | 0.01                           | 61.8                   | 50.2                                     | Beads-on-string                                   |
|                                  | 1,030,000         | 0.068               | 1.3                      | 229                             | 0.01                           | 62.1                   | 52.1                                     | Beads-on-string                                   |

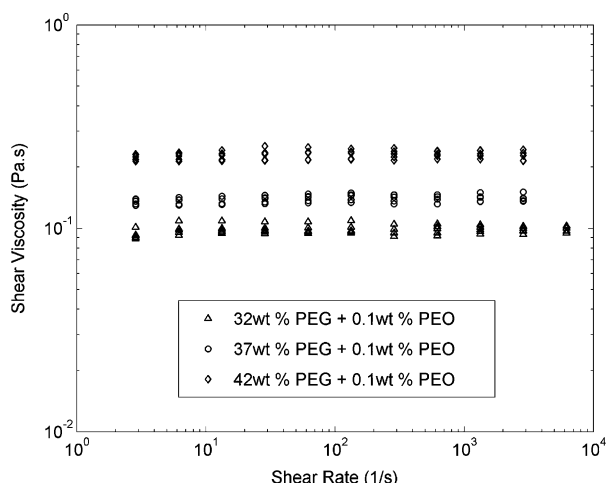


Fig. 2. The shear-viscosity of PEO/PEG solutions containing 0.1 wt % PEO. There are five solutions with different PEO molecular weights within each series (see Table 1 for details).

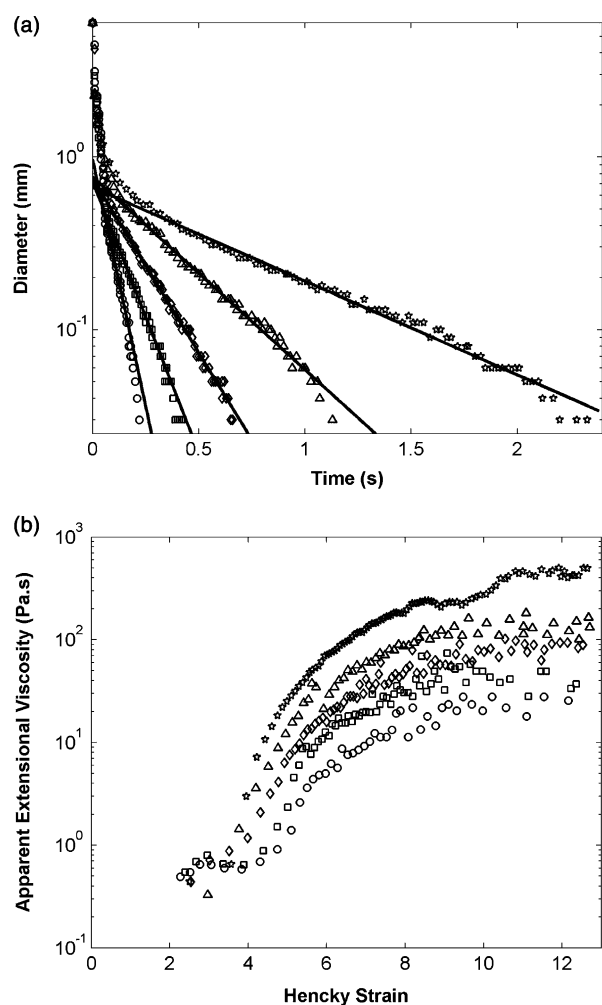


Fig. 3. Extensional properties of PEO/PEG solution (Series B1): (a) filament diameter evolution for the five different molecular weights of PEO. Solid lines are the best fits to Eq. (3). (b) Extensional viscosity. (○: 672 k, □: 772 k, ◇: 920 k, △: 954 k, ☆: 1030 k).

added PEO, the relaxation times were too short to determine by CaBER ( $\lambda_p < 0.005$  s).

### 3.2. Formation of beads-on-string morphology

During electrospinning, an electrically charged jet is emitted from the tip of the spinneret. Under appropriate operating conditions, as it accelerates in the external electric field, the jet experiences an instability that leads to whipping and stretching of the jet. Table 2 presents a typical set of processing conditions for Series B1. In general, lower electric field strengths are required to maintain steady spinning for more elastic solutions. The distance from the nozzle to the onset of whipping is also longer for more elastic solutions. When the jet dries and reaches the collector, it forms a solid fiber mat. However, for some spin solutions, only fibers exhibiting the ‘beads-on-string’ morphology were obtained. Fig. 4 shows the morphology of the electrospun fibers from solutions in Series B1. It illustrates the effect of increasing elasticity on the fiber morphology with increasing molecular weight of PEO. For fluids with low relaxation time or low extensional viscosity, the formation of ‘beads-on-string’ takes place.

The Rayleigh instability driven by the surface tension is the cause for the formation of ‘beads-on-string’ structure in these cases. This instability can be slowed down or suppressed by the viscoelastic behavior of the fluid jet. One way to quantify this competition between the instability growth and the viscoelastic response is to compare the respective time scales. The viscoelastic response of a polymer fluid can be described by its relaxation time,  $\lambda_p$ . The relevant time scale for the instability growth is the inverse of the instability growth rate. According to Chang, the maximum dimensionless growth rate of a viscoelastic jet  $\omega_{max}$  corresponding to the fastest growing Rayleigh instability is given by the following expression [42]

$$\omega_{max} = \frac{1}{2\sqrt{2Ca}(1 + 3S\sqrt{Ca/2})} \quad (4)$$

where  $S = 1/(1 + G\lambda_p/\mu_s)$  is the retardation number,  $\mu_s$  is the solvent viscosity,  $Ca = (\rho v^2)/(\sigma r_0^2)$  is the capillary number,  $r_0$  is the characteristic length,  $v = \mu_s/(S\rho)$  is the characteristic velocity,  $\rho$  is the density,  $\sigma$  is the surface tension, and  $G$  is the elastic modulus of the fluid. We introduce the ratio of the

Table 2  
Processing conditions for Series B1

|          | PEO $M_w$ (g/mol) | Electric field strength (V/m) | Electric current on jet ( $10^{-9}$ A) | Flight distance before the onset of whipping (mm) | Jet thinning exponents |
|----------|-------------------|-------------------------------|--|---|------------------------|
| B1:      | 672,000           | $6.00 \times 10^4$            | 72.9                                   | 50  | -0.27                  |
| 37 wt%   | 772,000           | $3.13 \times 10^4$            | 45.8                                   | 64  | -0.30                  |
| PEG, 0.1 | 920,000           | $3.07 \times 10^4$            | 51.7                                   | 82  | -0.32                  |
| wt%      | 954,000           | $1.34 \times 10^4$            | 32.1                                   | 150   | -0.37                  |
| PEO      | 1,030,000         | $1.50 \times 10^4$            | 20.0                                   | 210   | -0.45                  |

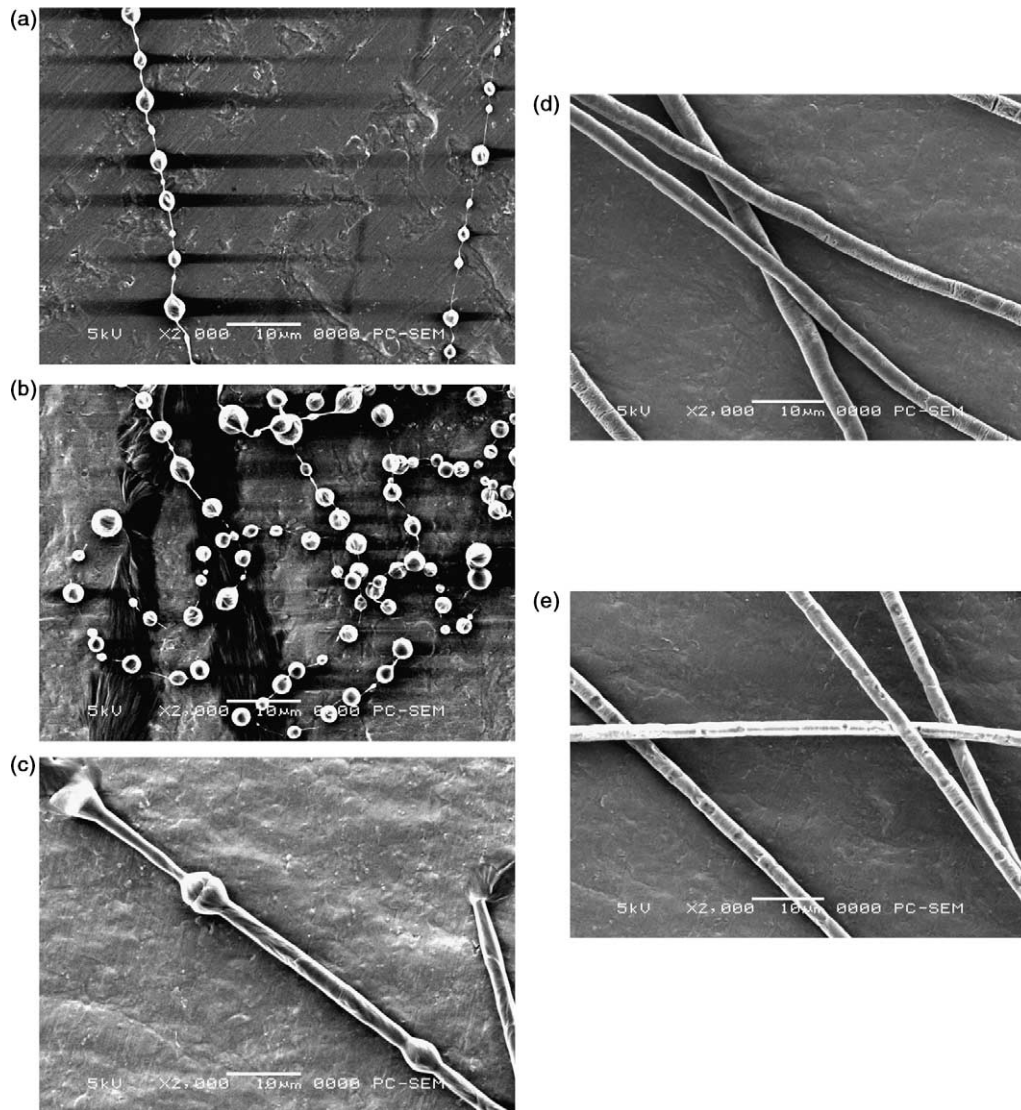


Fig. 4. Deborah number and electrospun fiber morphologies for Series B1: (a) 672 k,  $De=1.2$ , 'beads-on-string' (b) 772 k,  $De=2.3$ , 'beads-on-string' (c) 920 k,  $De=3.7$ , 'beads-on-string' (d) 954 k,  $De=6.1$ , uniform fibers (e) 1030 k,  $De=13.1$ , uniform fibers.

fluid relaxation time and instability growth time

$$De = \frac{\lambda_p \omega_{\max}}{t^*} \quad (5)$$

also known as the Deborah number,  $De$ . Here  $t^* = r_0^2/\nu$  is the characteristic time, by which  $\omega_{\max}$  was rendered dimensionless in Eq. (4) [42]. We take the initial radius of the electrified jet ( $r_0 = 0.8$  mm) as the characteristic length. If the fluid relaxation time is much greater than the instability growth time ( $De \gg 1$ ), the capillary forces responsible for the Rayleigh instability activate the elastic response, which in turn delays the jet breakup. In this case capillary forces do not break the jet into the drops like in the case of Newtonian fluids, but gradually squeeze the fluid into the 'beads' connected by highly elastic 'strings'. Only if the instability is completely suppressed by elastic forces (conditions for which are discussed later) or arrested at a very early stage of instability growth (very high  $De$ ) will the resulting fibers have the appearance of being uniform. The Deborah numbers for all our PEO/PEG test fluids

are well above unity. None of the PEO/PEG fluid jets broke up into droplets during electrospinning; only beads-on-strings or uniform fibers were formed. Without added PEO, the PEG solutions formed only droplets; their Deborah numbers are estimated to be less than 0.2.

The fluids that have large Deborah numbers favor formation of uniform fibers over the 'beads-on-string' morphology. The results are summarized in Fig. 5 for all solution series as functions of  $De$  and the dimensionless viscous number (or the Ohnesorge number,  $Oh = \mu/(\rho\sigma R_0)^{1/2}$ ). The Ohnesorge number demonstrates no visible correlation with bead-on-string or uniform fibers, thus demonstrating that the Newtonian shear viscosity does not determine the fiber morphology. On the other hand, there is a strong dependence of fiber morphology on the elastic effect; for  $De$  above 6, uniform fibers are generally observed. As the fluid relaxation time is the major parameter characterizing the fluid elasticity, we see a strong indication of the elasticity as the material property controlling the fiber morphology. To the best of our knowledge, our spin solutions

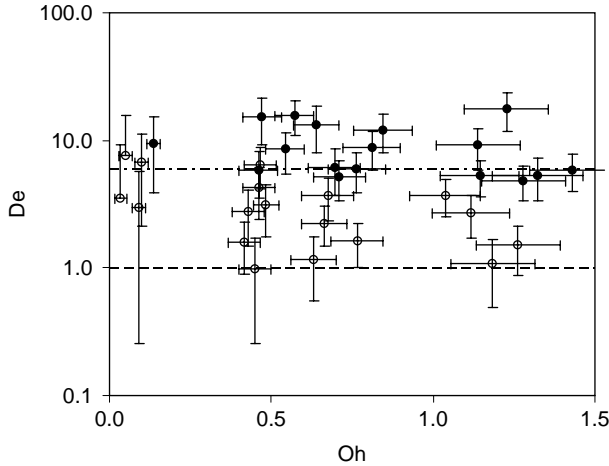


Fig. 5. Dependence of fiber morphology on the Deborah number and the Ohnesorge number for all solutions: solid symbols are uniform fibers; open symbols are ‘beads-on-strings’. The dot-dashed line corresponds to  $De=6$ .

have the lowest shear viscosities of any solutions reported to form uniform electrospun fibers.

### 3.3. Suppression of the Rayleigh instability and formation of uniform fiber

Next, we discuss the role of the build up of the elastic stress on the jet, caused by the extensional deformation, in suppressing the Rayleigh instability. The charged fluid jet exiting the spinneret travels in a straight path for a short distance (the ‘steady jet’) before it undergoes whipping instability. In this steady jet regime, it undergoes almost pure extensional deformation that can trigger the elastic response of the fluid and cause a build up of the elastic stresses in the jet. In principle, such elastic response can completely suppress the Rayleigh instability. The critical stress in the jet necessary for a complete suppression of the Rayleigh instability can be calculated theoretically. The actual elastic stress in the jet can be estimated from our knowledge of the jet profile. Below we analyze the correlation between these stresses to demonstrate the role of elasticity in suppression of the Rayleigh mode and in the formation of the uniform fibers.

Using macrophotography, we imaged the jet radius as a function of position,  $h(z)$ , from the nozzle to a point close to the onset of instability, where the jet is too small to be captured by the camera. Initially, the jet contracts rapidly near the exit of the nozzle. Then it thins down slowly and its profile can be described by a power law with a negative exponent ranging from  $-0.27$  for the least elastic fluids to  $-0.45$  for the most elastic fluids (Fig. 6). The jet radius,  $h_i$ , is then obtained by extrapolation to the distance from the nozzle where the whipping instability was observed to begin. For more elastic fluids the jet thins more slowly, and travels farther before it undergoes whipping instability. Interestingly, we observe that all of the jets in this work start whipping when their radii reach 10–20  $\mu\text{m}$ . From the data on jet diameter, we calculate the

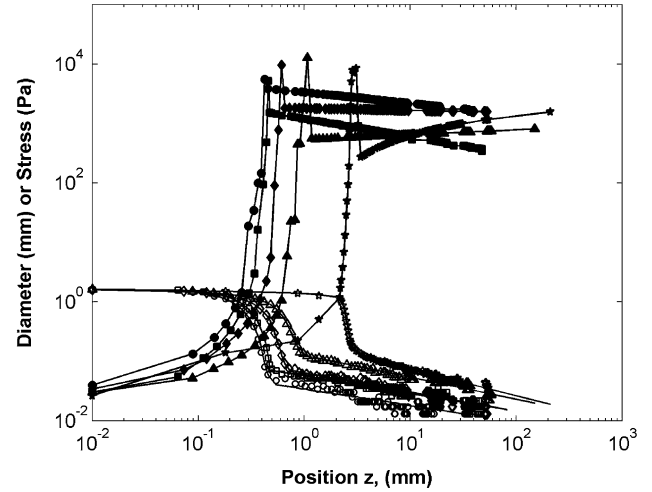


Fig. 6. Jet profiles and stress profiles as functions of position along steady jet, for Series B1. ( $\circ$ : 672 k,  $\square$ : 772 k,  $\diamond$ : 920 k,  $\triangle$ : 954 k,  $*$ : 1030 k). Jet diameter  $h(z)$ : unfilled symbols; extensional stress  $\tau_{zz}$ : filled symbols.

Hencky strain rate at any point along the steady jet

$$\dot{\epsilon} = \frac{-2Q}{\pi h(z)^3} \frac{\partial h(z)}{\partial z} \quad (6)$$

where  $Q$  is the volumetric flow rate. The Hencky strain in the steady jet is then determined by integration of Eq. (6). The extensional stress in the jet is estimated to be

$$\tau_{zz} \approx \dot{\epsilon} \eta_{\text{ext}} \quad (7)$$

where  $\eta_{\text{ext}}$  is the corresponding extensional viscosity at the same Hencky strain as observed in the CaBER experiment. Fig. 6 also shows that there is a large stress in the jet immediately near the exit of the nozzle that stretches the jet significantly and can trigger the viscoelastic response. For the less elastic fluids, this initial stress relaxes downstream, away from the nozzle. This relaxation is slower for more elastic fluids, and in some cases, the stress even continues growing along the jet.

To quantify this competition between the instability growth and the viscoelastic response, we use the dimensionless dispersion relation derived by Chang et al. for axisymmetric instability in a cylindrical jet of a viscoelastic fluid [42]

$$\omega^2 + 3S\alpha^2\omega - \alpha^2 \left( \frac{h}{2Ca} - \hat{\tau}_{zz} \right) + \frac{\alpha^4 h}{2Ca} = 0 \quad (8)$$

where  $\omega$  is the instability growth rate,  $\alpha$  is the instability wavelength,  $h$  is the jet radius, and  $\hat{\tau}_{zz}$  is the dimensionless stress along the jet axis. From this equation, one obtains the expression for the instability growth rate as a function of the instability wavelength and the extensional stress in the jet:

$$\omega = -\frac{3S\alpha^2}{2} \pm \frac{\sqrt{9S^2\alpha^4 - \alpha^2 4\hat{\tau}_{zz} + \frac{2h}{Ca}\alpha^2(1-\alpha^2)}}{2} \quad (9)$$

If the discriminant of Eq. (8) is positive, the above expression for the growth rate may be positive and real, corresponding to unstable modes. This condition is satisfied if

the extensional stress is not too large. The spectra of the Rayleigh instability growth rate and the Rayleigh instability wavelength at several different values of extensional stress are shown in Fig. 7. For the jet to be unstable with respect to Rayleigh instability, the extensional stress due to elastic response must be less than the critical value given by the following expression:

$$\hat{\tau}_{zz, \text{critical}} = \frac{h}{2Ca} \quad (10)$$

From the absence of any ‘beads-on-string’ observations in photographs of the straight jets, we know that the Rayleigh instability, if it occurs, does so after the onset of whipping. Furthermore, given the extension of the jet that occurs in the whipping instability, it is reasonable to conclude that the extensional stress in the jet is lower prior to the onset of whipping than after. Therefore, an elastic jet in which the Rayleigh instability is suppressed up to the onset of whipping will likely remain uniform throughout the subsequent stretching and drying processes; the ‘beads-on-string’ formation must take place in the whipping region under the condition that the extensional stress remains below the critical value even as the jet whips. To determine whether the stress near the onset of whipping is at or above the critical value to suppress the Rayleigh instability, we evaluate the stress at the axial location where the whipping instability is observed to begin, and plot this versus the theoretical critical stress evaluated using Eq. (7) and the radius of the steady jet at the onset of whipping,  $h_i$ . Fig. 8 shows the actual stress on the jet at the onset of whipping versus the critical stress needed to arrest the growth of the Rayleigh instability, for all the PEG+PEO solutions. For the jets that have stress values comparable to or greater than the critical value, the formation of uniform fibers is indeed observed. On the other hand, the ‘beads-on-string’ morphology is prevalent for those jets whose axial stress estimated at the onset of whipping is lower than the critical value. This result

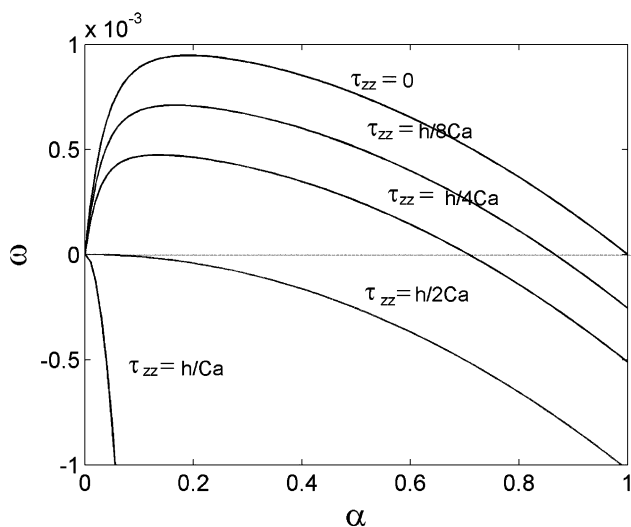


Fig. 7. Plots of  $\omega$  versus  $\alpha$  at several different stresses for one of the PEG+PEO solutions at onset of whipping (37 wt% PEG+0.1 wt% PEO  $M_w = 1030$  k,  $S = 0.215$ ,  $Ca = 758$ ,  $h = 1$ ).

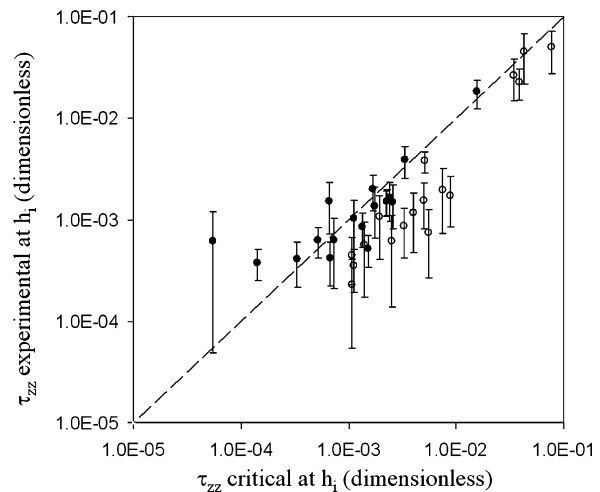


Fig. 8. Plot of the extensional stress on the jet at the onset of the whipping instability versus the critical stress for all PEG+PEO solutions. (Stress is in  $S\rho v^2/h_i^2$  units.) Solid symbols are uniform fibers; open symbols are ‘beads-on-strings’.

confirms the importance of elasticity for generating the critical stress required to suppress the Rayleigh instability and thereby generate uniform fibers, rather than beads-on-string morphologies. It also suggests that the inequality  $2\hat{\tau}_{zz}Ca/h \geq 1$  offers a suitable criterion for the formation of uniform fibers (Fig. 8).

#### 4. Conclusions

We have investigated experimentally and theoretically the role of fluid elasticity in electrospinning. The use of Boger fluids for this investigation allowed us to evaluate the role of fluid elasticity independently of the other fluid material properties. Boger fluids exhibit Newtonian behavior under shear and thus their elasticity is purely extensional. Experimental solutions covering a broad range of elastic responses and relaxation times were obtained by adding small amounts of high molecular weight PEO to aqueous solutions of PEG.

All the PEO/PEG fluids used in this work led to the formation of bead-on-string structures or uniform fibers. Only the inelastic PEG solutions formed droplets. This observation correlates with the fact that the Deborah number, defined here as a ratio of fluid relaxation time to the instability growth time, was always greater than one for the PEO/PEG solutions used in the experiments, and less than one for the PEG solutions. In such cases, the initial growth of the capillary-driven Rayleigh instability, when it occurs, is always fast enough to trigger the elastic response of the fluid. As the beads grow, they remain connected by highly elastic ‘strings’ and do not experience the final breakup into individual droplets. Such behavior is also typical of uncharged jets of viscoelastic fluids. As these jets dry, they too exhibit the beads-on-string morphology. Notably, all of our 0.1 wt% PEO solutions exhibit values of  $c[\eta]$  less than 1.0.

In addition to capillary stresses, electrospun jets also exhibit axial stresses due to action of the external electric field on

the charged jet and to repulsion between charges on the jet. If extensional deformation due to either of these electrical stresses is fast compared to the inverse of the fluid relaxation time, it will cause a buildup of the elastic stress in the fluid jet. As was shown theoretically, if this stress reaches a critical value, it can suppress the Rayleigh instability completely and lead to formation of uniform fibers in electrospinning. In this work, the elastic stress along the jet was estimated based on the information about the jet profile and CaBER data. Comparison of the experimentally determined elastic stresses with theoretically derived critical stresses supports the idea that uniform fibers can be formed during electrospinning as a result of the complete suppression of the Rayleigh instability, made possible by the build-up of elastic stress due to electrical forces.

In closing, we emphasize that all of our experimental fluids had concentrations of PEG and PEO below that where any entanglement transition is observed and shear viscosities less than 0.30 Pa s. The role of such fundamental fluid properties as shear viscosity and presence of entanglements in setting the morphology of the fibers produced in electrospinning has been discussed in Refs. [14,18,19]. Our results clearly indicate that the presence of entanglements is not required for the formation of uniform fibers. We also observed no correlation between the Newtonian viscosity of the fluid and the fiber morphology. These observations point to the fact that fluid elasticity, as measured by relaxation time, is the essential property controlling the morphology of the fibers produced by electrospinning.

### Acknowledgements

We are grateful to Dr G.H. McKinley for numerous valuable discussions on extensional rheology and the CaBER. This research was supported by the US. Army through the Institute for Soldier Nanotechnologies, under Contract DAAD-19-02-D-0002 with the US. Army Research Office. The content does not necessarily reflect the position of the Government, and no official endorsement should be inferred.

### References

- [1] He CH, Gong J. *Polym Degrad Stab* 2003;81:117.
- [2] Shao C, Kim H-Y, Gong J, Ding B, Lee D-R, Park S-J. *Mater Lett* 2003; 57:1579.
- [3] Boland ED, Matthews JA, Pawlowski KJ, Simpson DG, Wnek GE, Bowlin GL. *Front Biosci* 2004;9:1422.
- [4] Lee SW, Belcher AM. *Nano Lett* 2004;4:387.
- [5] Gibson P, Schreuder-Gibson H, Rivin D. *Colloids Surf, A* 2001;187:469.
- [6] Liu HQ, Kameoka J, Czaplewski DA, Craighead HG. *Nano Lett* 2004;4: 671.
- [7] Wang X, Kim Y-G, Drew C, Ku B-C, Kumar J, Samuelson L. *Nano Lett* 2003;4:331.
- [8] Wang M, Singh H, Hatton TA, Rutledge GC. *Polymer* 2004;45:5505.
- [9] Acatay K, Simsek E, Ow-Yang C, Menciloglu Y. *Angew Chem, Int Ed Eng* 2004;43:5210.
- [10] Ma ML, Hill RM, Lowery JL, Fridrikh SV, Rutledge GC. *Langmuir* 2005; 21:5549.
- [11] Ma M, Mao Y, Gupta M, Gleason KK, Rutledge GC. *Macromolecules* 2005;38:9742.
- [12] MacDiarmid AG, Jones Jr. WE, Norris ID, Gao J, Johnson Jr. AT, Pinto NJ, et al. *Synth Metal* 2001;119:27.
- [13] Fong H, Chun I, Reneker DH. *Polymer* 1999;40:4585.
- [14] Lee KH, Kim HY, Bang HJ, Jung YH, Lee SG. *Polymer* 2003;44:4029.
- [15] Gupta P, Elkins C, Long TE, Wilkes GL. *Polymer* 2005;46:4799.
- [16] Norris ID, Shaker MM, Ko FK, MacDiarmid AG. *Synth Metal* 2000;114: 109.
- [17] Jin H-J, Fridrikh SV, Rutledge GC, Kaplan DL. *Biomacromolecules* 2002;3:1233.
- [18] McKee MG, Elkins CL, Long TE. *Polymer* 2004;45:8705.
- [19] McKee MG, Park T, Unal S, Yilgor I, Long TE. *Polymer* 2005;46:2011.
- [20] Shenoy SL, Bates WD, Wnek G. *Polymer* 2005;46:8990.
- [21] Shenoy SL, Bates WD, Frisch HL, Wnek GE. *Polymer* 2005;46:3372.
- [22] Boger DV. *J Non-Newton Fluid Mech* 1977;3:87.
- [23] Dontula P, Macosko CW, Scriven LE. *AICHE J* 1998;44:1247.
- [24] Goldin M, Yerushalmi J, Pfeffer R, Shinnar R. *J Fluid Mech* 1969;38:689.
- [25] Funada T, Joseph D. *J Non-Newton Fluid Mech* 2003;111:87.
- [26] Bousfield DW, Keunings R, Marrucci G, Denn MM. *J Non-Newtonian Fluid Mech* 1986;21:79.
- [27] Hohman MM, Shin YM, Rutledge GC, Brenner MP. *Phys Fluids* 2001;13: 2201.
- [28] Hohman MM, Shin YM, Rutledge GC, Brenner MP. *Phys Fluids* 2001;13: 2221.
- [29] Reneker DH, Yarin AL, Fong H, Koombhongse S. *J Appl Phys* 2000;87: 4531.
- [30] Spivak AF, Dzenis YA, Reneker DH. *Mech Res Commun* 2000;27:37.
- [31] Yarin AL, Koombhongse S, Reneker DH. *J Appl Phys* 2001;89:3018.
- [32] Magarvey RH, Outhouse LE. *J Fluid Mech* 1962;13:151.
- [33] Huebner AL. *J Fluid Mech* 1969;38:679.
- [34] Zeng J, Hou H, Schaper A, Wendorff JH, Greiner A. *e-Polymers* 2003; 009:1.
- [35] Theron SA, Zussman E, Yarin AL. *Polymer* 2004;45:2017.
- [36] McKee MG, Wilkes GL, Colby RH, Long TE. *Macromolecules* 2004;37: 1760.
- [37] Porter R, Johnson J. *Trans Soc Rheol* 1962;6:107.
- [38] Devanand K, Selser JC. *Macromolecules* 1991;24:5943.
- [39] McKinley G, Sridhar T. *Annu Rev Fluid Mech* 2002;34:375.
- [40] Anna SL, McKinley GH. *J Rheol* 2001;45:115.
- [41] Rodd LE, Scott TP, Cooper-White JJ, McKinley G. *Appl Rheol* 2005;15: 12–27.
- [42] Chang HC, Demekhin EA, Kalaidin E. *Phys Fluids* 1999;11:1717.